Dual-functional Gum Arabic Binder for Silicon Anodes in Lithium Ion Batteries

Min Ling[a,b], Yanan Xu[c], Hui Zhao[b], Xingxing Gu[a], Jingxia Qiu[a], Sheng Li[a], Mingyan Wu[b], Xiangyun Song[b], Cheng Yan[c], Gao Liu[b] and Shanqing Zhang[a*]*

[a] Centre for Clean Environment and Energy, Environmental Futures Research Institute and Griffith School of Environment, Gold Coast Campus, Griffith University QLD 4222, Australia. E-mail: s.zhang@griffith.edu.au
[b] Environmental Energy Technologies Division, Lawrence Berkeley National Laboratory, Berkeley, California 94720, USA. E-mail: gliu@lbl.gov
[c] School of Chemistry, Physics and Mechanical Engineering, Queensland University of Technology, Brisbane, QLD 4001, Australia.

Keywords: Fibers reinforcement, high capacity silicon electrodes, water-based binders, lithium-ion batteries

Abstract: Si has attracted enormous research and manufacturing attention as an anode material for lithium ion batteries (LIBs) because of its high specific capacity. The lack of a low cost and effective mechanism to prevent the pulverization of Si electrodes during the lithiation/delithiation process has been a major barrier in the mass production of Si anodes. Naturally abundant gum arabic (GA), composed of polysaccharides and glycoproteins, is applied as a dual-function binder to address this dilemma. Firstly, the hydroxyl groups of the polysaccharide in GA are crucial in ensuring strong binding to Si. Secondly, similar to the function of fiber in fiber-reinforced concrete (FRC), the long chain glycoproteins provide further mechanical tolerance to dramatic volume expansion by Si nanoparticles. The resultant Si anodes present an outstanding capacity of ca. 2000 mAh/g at a 1 C rate and 1000 mAh/g at 2 C rate, respectively, throughout 500 cycles. Excellent long-term stability is demonstrated by the maintenance of 1000 mAh/g specific capacity at 1 C rate for over 1000 cycles. This low cost, naturally abundant and environmentally benign polymer is a promising binder for LIBs in the future.

1. Introduction

In the development and implementation of sustainable energy technologies, lithium ion batteries (LIBs) are among the most important and attractive power sources serving as the dominant power sources for portable electronics, electrical vehicles and smart energy utility grids. Silicon (Si) is an attractive anode material candidate due to its superior theoretical specific capacity of ca. 4200 mAh/g assuming full lithiation to $Li_{4.4}Si$, which is an order of magnitude higher than that of conventional graphite anodes [1, 2]. Si anodes are however, still far from commercialization due to significant challenges such as substantial volume change (ca. 300%) during lithiation/delithiation processes [3-6]. This volume change causes high stress and even electrode pulverization in the electrode laminate, which eventually breaks the integrity of the electrode, resulting in rapid degradation of the electrode and short cycle life. Tremendous efforts have been devoted to addressing this issue. Compared with complicated and costly Si nano-manipulation processes [7-10], the engineering of polymer binders is the most promising and practical approach because it can tune the mechanical and electronic characteristics of the binders. To date, polymers with tailored electronic properties, binding strength, wettability, flexibility and even self-healing abilities have been proposed to replace conventional polyvinylidene difluoride (PVdF) binder [11-17].

Besides the strong binding capability, an excellent polymer binder should guarantee the electronic and ionic conductivity at the active material particles surface/electrolyte interface [14]. The thermal and electrochemical stabilities of the polymer binder are also of primary importance to guarantee battery performance. In terms of the mechanical properties (particle/particle cohesion and laminate/current collector adhesion), the state-of-the-art roll-to-roll lamination process in industry specifically requires a flexible and ductile polymer binder/electrode laminate to avoid crack generation and propagation, especially in the case of high volume change Si electrodes [18]. In strong contrast with research into electro-active

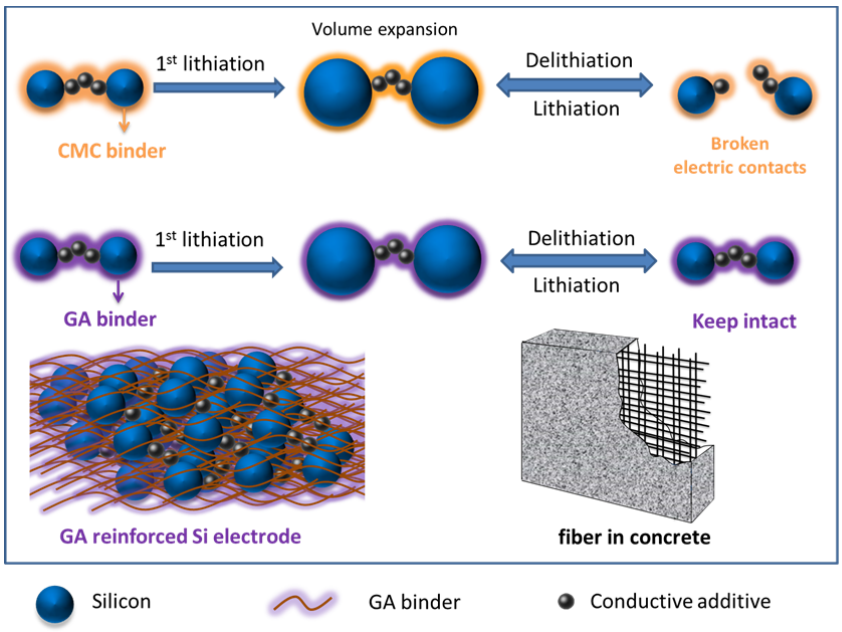

Figure 1. Schematics of the concept to address volume change issue in battery materials. GA with dual functionality could keep both the strong chemical bonding and the ductile property to tolerate the expansion during lithiation/delithiation processes.

materials, the lack of significant progress in binders impedes the industrialization of Si anodes [19, 20].

In the 21st century, the adoption of environmentally friendly sustainable materials and industrial processes prevails in the research and industrial world. Naturally carboxyl methylated cellulose (CMC) polymer binder attracted the initial attention in this regard as it opens up water-based process for electrode manufacture [21, 22]. Limited success has been achieved due to the single function of the CMC binder – the hydroxyl functional groups afford the chemical bonding with Si based materials, mainly due to CMC could not handle such a dramatic volume change resulting in physical contact breaks (see Figure 1). Herein, we apply gum arabic (GA) polymer as a dual function binder utilizing the concept of fiber-reinforced concrete (FRC) in LIB electrode fabrication. It is well-established that the fibers reinforce the rigidity and flexibility in the "concrete" laminate [23-26].

GA is widely produced in nature and has many applications (*eg.* emulsifier and thickening

agent in food, binder for painting and printmaking, *etc.*) [27]. Essentially, GA is a complex mixture of polysaccharides and glycoproteins. Polysaccharides are long carbohydrate monosaccharide's units with abundant hydroxyl groups. Glycoproteins are proteins that contain long oligosaccharide chains covalently attached to polypeptide side-chains (See Figure S1) [28, 29]. As shown in Figure 1, the functional groups on polysaccharides provide the physiochemical and chemical binding while the long spiral glycoprotein chain behaves like the fibers in concrete [17, 30, 31]. Fibers for reinforcement in laminate can be classified into two categories: (i) low modulus, high elongation fibers such as nylon, polypropylene and polyethylene. This type of fibers could primarily enhance the energy absorption of composites in the post-cracking stage (as glycoprotein in GA) and (ii) high modulus and mechanical strength fibers such as steel, glass and asbestos that could enhance the strength and the toughness of the composites [23-26, 32-36]. The natural gum-derived polymer GA is applied as the binder to enhance the tolerance to cracking from volume expansion in Si anode materials.

2. Result and discussion

In this work, GA is used as the green binder to immobilize Si electrode materials and conductive additives onto the copper current collector by forming a Si and GA laminate (Si@GA). Si and CMC (Si@CMC) are prepared under identical conditions as a control sample. The mechanical properties of the resultant laminates are quantified using nano-scratch and nano-indentation tests. The normal force in the scratch test is set to 500 μN and the scratch length is set to 10 μm. During the scratch tests, lateral force is real-time recorded and the friction coefficient can be calculated from it with known applied normal force, as shown in Figure 2a. The average friction coefficient of Si@GA electrode is higher than that of CMC. Moreover, the friction coefficient of Si@GA remains more constant along the whole scratch process even after 200 cycles.

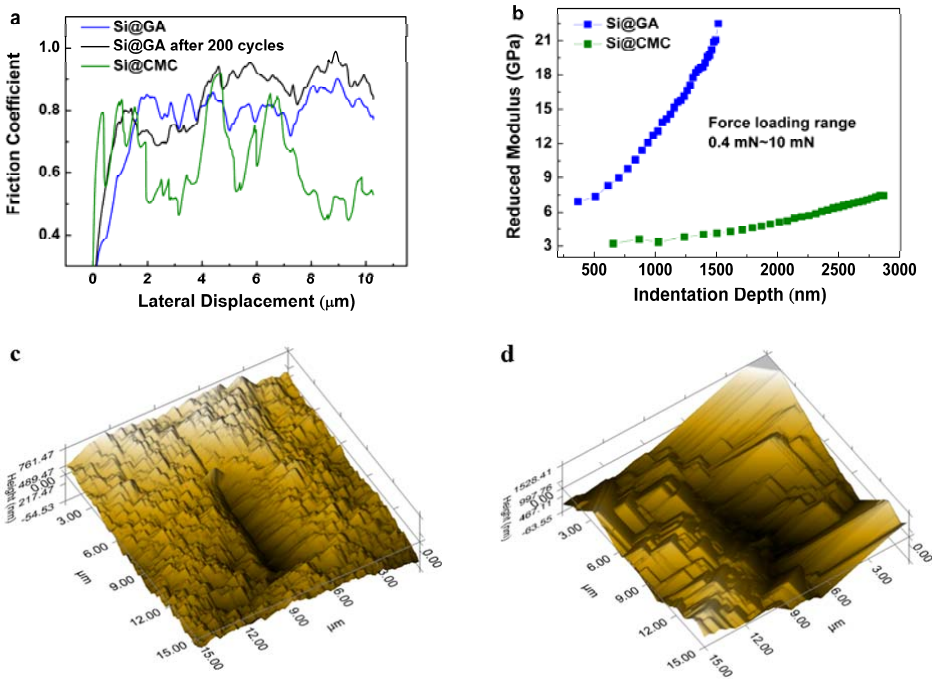

Figure 2. (a) The nano-scratch tests for Si@GA, Si@GA after 200 cycles and Si@CMC electrodes. (b) The nano-indentation tests represent the average reduced modulus variation with different indentation depth for GA/Si and CMC/Si electrodes. (c) 3D in-situ SPM image of Si@GA after nano-scratch tests. (d) 3D in-situ SPM image of Si@CMC electrode after nano-scratch tests.

Scanning Probe Microscopy (SPM) is used to obtain the 3D in-situ images of nano-scratch impressions, as shown in Figure 2c and d. The higher and stable friction values of the Si@GA electrode imply better mechanical properties including the binding force, than the Si@CMC electrode. Furthermore, the SPM of the electrodes after a scratch test between Si@GA and Si@CMC electrodes show drastic differences. The scratch track of the GA based electrode is smooth, with limited cracks of the laminate. In contrast, the CMC based electrode shows irregular distribution patterns on its scratch track. Because the scratch test simulates the stress induced by the volume change, this result demonstrates that GA binder is more compliant and might provide greater tolerance to volume change than CMC due to the FRC effects.

Nano-indentation tests on Si@GA and Si@CMC electrodes are undertaken with the force vary from 0.4 mN to 10 mN. A partial unload function was adopted in the

tests to obtain the variation of reduced modulus *Er* and hardness *H*. The indentation depth *Er* is a combined modulus of the indenter and the specimen and is given by:

$$\frac{1}{E_r} = \frac{(1-v^2)}{E} + \frac{(1-v'^2)}{E'}$$

Where, E and v are the Young's modulus and Poisson's ratio of the specimen respectively, E' and v' are the elastic modulus and Poisson's ratio of the indenter respectively. For a standard diamond indenter probe, E' is 1140 GPa and v' is 0.07. To ensure representativeness of experimental results, at least seven indentations were conducted at different locations on each sample. The averaged reduced modulus E_r and hardness H variation with different indentation depth for Si@GA and Si@CMC electrodes are shown in Figure 2b. The higher reduced modulus value for Si@GA represent much better binding force among the Si particles compared with that of CMC. Materials such as glass, sugar and rosin crystals have reduced modulus values as high as the Si@GA electrode, but are quite brittle. Hence, measurement of hardness H is evaluated here by the mean contact pressure at full load and is given by:

$$H = \frac{P_{max}}{A}$$

Where, A is the projected area of contact (as distinct from the actual curved area of contact), P_{max} is the maximum load. Interestingly, in the GA binder system, the higher H value compared with Si@CMC (See Figure S2a) implies higher ductile property and energy absorb ability, which differs from brittle glass and sugar crystals. The detailed indentation process profiles are also included in the supplementary information (see Figure S2b and c) [15, 37, 38].

High Li^+ ionic conductivity will facilitate the fast ion transport especially beneficial for high rate operation [39]. With regard to the ionic conductivity of the polymer binder, the electrolyte uptake is important for allowing facile Li^+ transportation through the polymer binder to the active material [12]. The high electrolyte uptake is beneficial for high Li^+ diffusion efficiency and subsequently facilitates the high capacity and better power

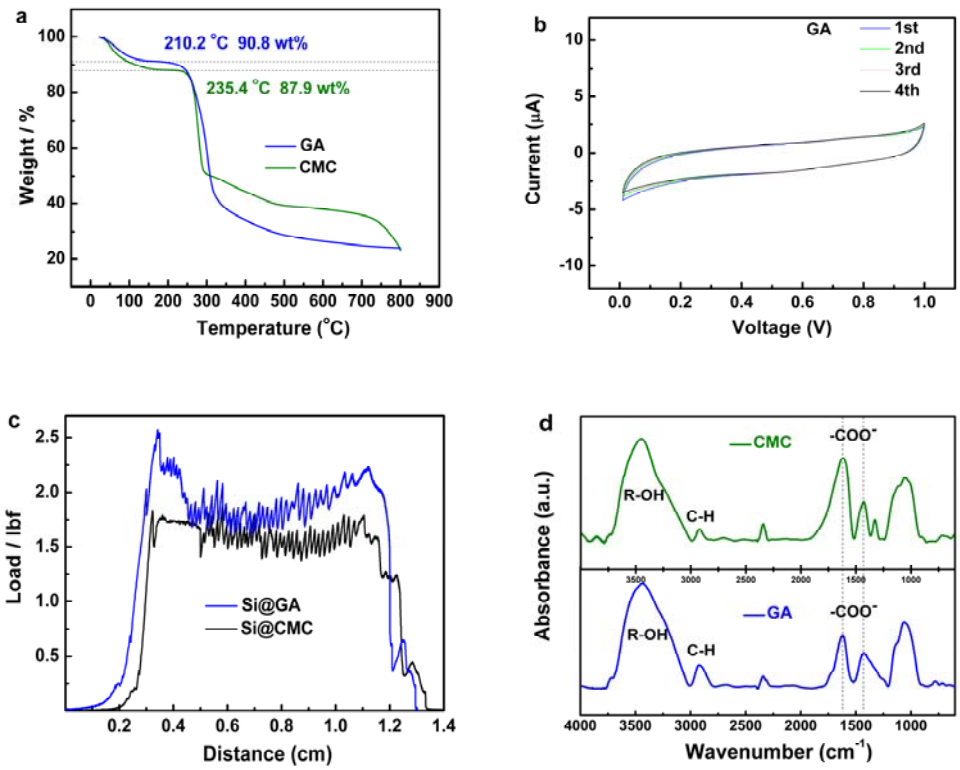

Figure 3. (a) TGA plots of GA and CMC polymer binders in the nitrogen atmosphere with the ramp 5 °C/min to 800 °C. (b) CV measurements evaluating the electrochemical stability of the GA polymer binders at a scan rate of 0.2 mV/s over the potential window of 0.01-1.00 V. (c) Peeling test of Si electrodes using GA and CMC binders. (d) FTIR of GA and CMC polymer binders.

performance of the Si electrode. In the GA binder system, the electrolyte uptake is accounting for ca. 19.5 wt% of its final weight, which is higher than the CMC's uptake percentage (ca. 12.6 wt%) in the electrolyte (See Figure S3).

The thermal stability for GA is a necessary condition for battery performance [16]. The thermal stability of the natural binders is examined using thermogravimetric analysis (TGA) ramping up to 800 °C at the rate of 5 °C/min to determine the water content and the carbonization temperature of the polymer binders with SiO_2 as a reference. The thermal gravimetric analysis revealed that 9.2 wt% and 2.1 wt% water is adsorbed by the GA and

CMC binders, respectively. (See Figure 3a) The steep curves show the carbonization process until 800 ^{o}C with the initiation temperature of ca. 210 ^{o}C for GA and ca. 235 ^{o}C for CMC.

The electrochemical behaviour of GA is evaluated through cyclic voltammetry (CV) at 0.2 mV/s (See Figure 3b). The CV profile demonstrates that GA is electrochemically stable in the anode working voltage range of 0.01-1V [40-42]. This inert electrochemical property during the 0.01-1 V range guarantees that the GA binder will not impede the lithiaion/delithiation processes.

To allow free electron transfer, a primary requirement of polymer binders in LIBs is to enable particle/particle cohesion and electrode laminate/current collector adhesion.[41] Low adhesion in electrodes leads to delamination of active materials from the current collector and ultimately causes significant capacity loss during repeated charge/discharge cycles [31, 40, 43]. The adhesion strength can be quantified via peel test as shown in Figure 3c. The Si@CMC laminates can persist on the current collector with no cracks or delamination observed, which is consistent with the literature [13, 44]. Moreover, Si@GA electrode performs even better than CMC through the entire adhesion test affording ca.0.3 pounds more peel force than CMC. The sufficient adhesion between electrode laminate and current collector ensures the electron collection from the circuit.

Hydroxyl and carboxylic functional groups contribute to improved cycle lifetime. Polyacrylic acid (PAA), CMC and alginate binders are reported as binders for Si based materials, all taking advantages of the hydroxyl or carboxyl functional groups. These functional groups can be directly verified by Fourier Transform Infrared (FTIR) spectroscopy. Figure 3d shows the FTIR spectra of the binder polymers. The strong and wide absorption peaks centred at ca. 3400 cm^{-1} suggests the abundant –OH functional groups within GA and CMC polymers, which are different to the inert PVDF binder. Two strong bands at 1620 cm^{-1} and 1430 cm^{-1} are due to asymmetric and symmetric stretching vibrations of the carboxylic acid salt $–COO^{-}$ of the GA and CMC [45]. It is estimated that the functional groups in the GA

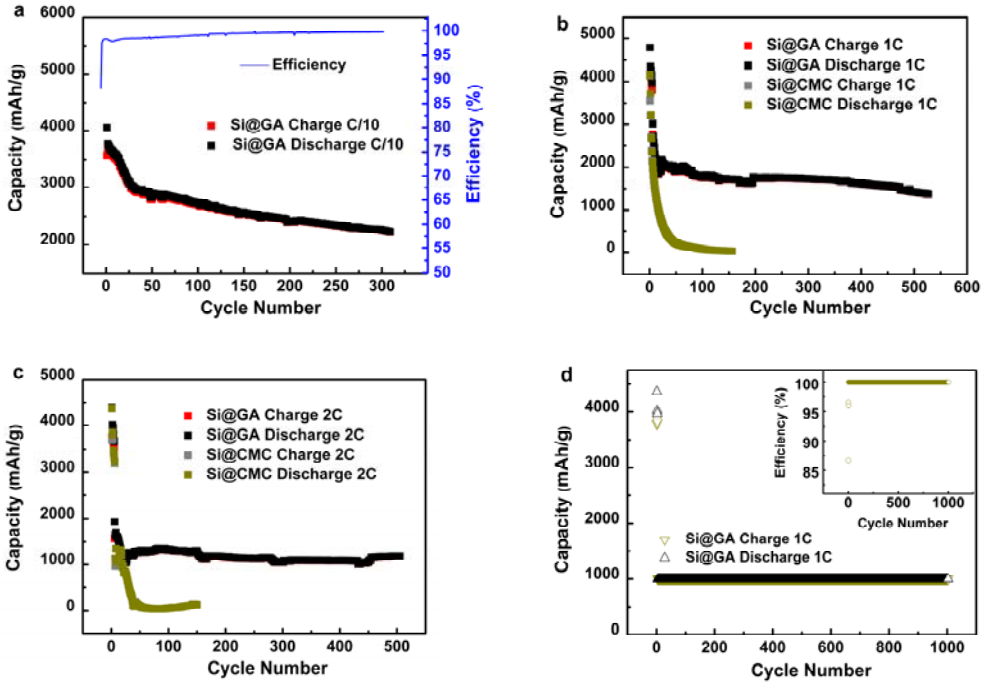

Figure 4. Electrochemical performance of Si@GA and Si@CMC electrodes (Si:C:binder = 2:1:1, wt %). Reversible Li-extraction capacity of the Si electrodes versus cycle number collected at (a) C/10 rate (420 mA/g), (b) 1 C rate (4200 mA/g) and (c) 2C (8400 mA/g) over the potential window of 0.01-1 V (versus Li/Li^+). (d) Reversible Li-extraction capacity and CE of the Si electrodes versus cycle number for Li insertion level fixed to 1000 mAh/g Si at 1 C rate (4200 mA/g) over the potential window of 0.01-1 V (versus Li/Li^+).

molecules can potentially adsorb onto the SiO_2 on the Si particle surfaces via hydrogen bonding when GA binder is mixed with Si and conductive additives in the slurry [13, 14, 31, 46].

The electrochemical performance of the Si@GA anode is tested in terms of galvanostatic discharge-charge cycling. Figure 4a shows the typical lithiation/delithiation profiles expected for Si combined with GA binder when at a current density of C/10 (420 mA/g). The first discharge and charge capacities are 4056 mAh/g and 3574 mAh/g, respectively, with an initial Columbic efficiency (CE) of 88.11 % (See Figure S4). All current

density and specific capacity calculations are based on the active mass of Si. The performance of Si@CMC is performed in Figure S5 for comparison. The irreversible capacity loss during the first cycle can be ascribed to the expected side reaction with the components of the electrolyte (slope from 0.7 V to 0.2 V). In the side reaction, solvent (EC, DEC and FEC) molecules and salt anions are reduced on the active materials surface, thus forming insoluble Li salt that precipitates to form a passivating film surface *i.e.*, solid electrolyte interface, (SEI), which prevents further reaction between the components of the electrolyte and the Si active material [47-49]. The initial reversible specific capacity is found to be higher than 3500 mAh/g which is close to the theoretical limit of Si electrodes (4200 mAh/g corresponding to the composition of the compound $Li_{4.4}Si$). After the first two cycles, the CE rapidly increases to ca. 99% and, remains highly stable throughout the cycles, indicating that the SEI layer remained intact and showed excellent reversible cycling after the surface reactions are completed. The reversible capacity after 100 cycles at C/10 is 2708 mAh/g, which corresponds to 75.7% retention of the initial capacity.

Figure 4b also shows that the Si@GA anode has a high discharge specific capacity of 1419 mAh/g after 500 cycles at the current density of 1C (4200 mA/g). Also, the CE remains steady at more than 99% indicating excellent reversibility (See Figure S6). When the current rate is increased to 2C (8400 mA/g), the specific capacity can be stable at ca. 1000 mAh/g throughout 500 cycles (Figure 4c and Figure S7). A slight decrease in the specific capacity is observed with cycling at C/10 and increasing the current rate from C/10 to 1C and then 2C. This decrease can be ascribed to limitations in Li^+ ions diffusion and electron transport through the porous anode active material grains. The charge-discharge cycling performed with Li insertion capacity limited to 1000 mAh/g show stable anode performance for more than 1000 cycles (Figure 4d and Figure S8). The SEM images in Figure S9 demonstrate the typical morphology before and after lithiation. The formation of solid electrolyte interface (SEI) film on the surface of Si@GA and Si@CMC electrodes (Fig S9c and d) could promote

the stability during the long-term cycling and facilitate the lithium ion conductivity. Furthermore, the SEM cross section for electrodes based on GA and CMC are demonstrated in Figure S10. With the synergistic effect of FRC on GA@Si, the thickness after lithiation is ca. 28 μm (ca.115 vol% increase) of the original thickness (ca. 13 μm). In stark contrast, the CMC@Si electrode has as high as ca. 184 vol% expansion (37 μm), which is responsible for the deterioration of electrode integrity and the decline of conductivity with the increase of cycling times.

Information on the incorporated Si anode materials is detailed through morphology observation and X-ray diffraction. (See Figure S11). The Si particle size distribution is ca. 200 nm diameter, with some particles reaching micron scale. All the XRD peaks correspond well with standard crystallographic data [International Centre for Diffraction Data (ICDD) File No. 001-0791]. The scanning electron microscopies (SEM) of the Si electrode based on GA are presented in Figure S11c and d. The uniform distribution of Si particles in the electrode is confirmed by the energy dispersive X-ray spectroscopy (EDS) presented in Figure S12. The Si electrodes are subjected to deep cycling (1 V-0.01 V) and then extracted for observation with EDS element analysis (See Figure S13). After 1000 cycles, the content of fluorine that decomposed from the electrolyte ($LiPF_6$) increases to ca. 45.6 atom%, which can be ascribed to the formation of solid electrolyte interface [50]. Based on the glycoprotein-reinforced Si electrode, the GA with polysaccharides is a promising binder for high specific capacity Si anode in LIBs.

3. Conclusion

A glycoprotein-reinforced Si electrode with high binding strength and ductility is achieved based on the gum arabic (GA) natural polymer binder. The concept of Fiber-reinforced concrete (FRC) is applied to the LIBs electrode fabrication process. There are two main benefits of GA are claimed as the origin of the performance enhancement: hydroxyl groups in polysaccharide increase the binding force and glycoproteins improve the mechanical

properties including the tolerance of volume expansion. The resultant anodes, *i.e.,* Si@GA anodes, have excellent adhesion to Si nanoparticles and current collector, ductility and more importantly, endure dramatic volume changes (up to 300%) of Si thereby prohibiting physical fracture during lithiation/delithiation processes. These outstanding properties stem from the concrete tensile structures formed by the abundant functional groups as well as the glycoprotein chain. A stable cycling performance is demonstrated at various C rates based on GA binder while a promising long-term performance of 1000 cycles is observed when limiting the specific capacity to 1000 mAh/g at 1 C.

Acknowledgements
This work is funded by the Australia Research Council and the Assistant Secretary for Energy Efficiency, Office of Vehicle Technologies of the U.S. Department of Energy (U.S. DOE) under contract no. DE-AC02-05CH 11231 under the Batteries for Advanced Transportation Technologies (BATT) Program. Electron microscopy experiments are conducted at the National Centre for Electron Microscopy (NCEM) located at Lawrence Berkeley National Laboratory (LBNL).
The manuscript is written through contributions of all authors. All authors have given approval to the final version of the manuscript. The authors declare no competing financial interest.

References

[1] Etacheri, V.; Marom, R.; Elazari, R.; Salitra, G.; Aurbach, D. Energy Environ. Sci. 4 (2011）3243.
[2] Goodenough, J. B.; Kim, Y. Chem. Mater. 22 (2010）587-603.
[3] Renganathan, S.; Sikha, G.; Santhanagopalan, S.; White, R. E. J. Electrochem. Soc. 157 (2010）A155-A163.
[4] Christensen, J.; Newman, J. J. Solid State Electrochem. 10 (2006）293-319.
[5] Fu, K.; Xue, L.; Yildiz, O.; Li, S.; Lee, H.; Li, Y.; Xu, G.; Zhou, L.; Bradford, P. D.; Zhang, X. Nano Energy 2 (2013）976-986.
[6] Ji, L.; Zheng, H.; Ismach, A.; Tan, Z.; Xun, S.; Lin, E.; Battaglia, V.; Srinivasan, V.; Zhang, Y. Nano Energy 1 (2012）164-171.
[7] Gauthier, M.; Mazouzi, D.; Reyter, D.; Lestriez, B.; Moreau, P.; Guyomard, D.; Roue, L. Energy Environ. Sci. 6 (2013）2145-2155.
[8] Du, C.; Gao, C.; Yin, G.; Chen, M.; Wang, L. Energy Environ. Sci. 4 (2011）1037-1042.
[9] Lee, J.-I.; Park, S. Nano Energy 2 (2013）146-152.
[10] Mukherjee, R.; Krishnan, R.; Lu, T.-M.; Koratkar, N. Nano Energy 1 (2012）518-533.
[11] Ling, M.; Qiu, J.; Li, S.; Zhao, H.; Liu, G.; Zhang, S. J. Mater. Chem. A 1 (2013）11543-11547.

[12] Wu, M.; Xiao, X.; Vukmirovic, N.; Xun, S.; Das, P. K.; Song, X.; Olalde-Velasco, P.; Wang, D.; Weber, A. Z.; Wang, L.-W.; Battaglia, V. S.; Yang, W.; Liu, G. J. Am. Chem. Soc. 135 (2013) 12048-12056.
[13] Ryou, M. H.; Kim, J.; Lee, I.; Kim, S.; Jeong, Y. K.; Hong, S.; Ryu, J. H.; Kim, T. S.; Park, J. K.; Lee, H.; Choi, J. W. Adv. Mater. 25 (2013) 1571-1576.
[14] Liu, G.; Xun, S.; Vukmirovic, N.; Song, X.; Olalde-Velasco, P.; Zheng, H.; Battaglia, V. S.; Wang, L.; Yang, W. Adv. Mater. 23 (2011) 4679-4683.
[15] Kovalenko, I.; Zdyrko, B.; Magasinski, A.; Hertzberg, B.; Milicev, Z.; Burtovyy, R.; Luzinov, I.; Yushin, G. Science 334 (2011) 75-79.
[16] Bonjae, K.; Hyunjung, K.; Younghyun, C.; Kyu Tae, L.; Nam-Soon, C.; Jaephil, C. Angew. Chem. Int. Ed. 51 (2012) 8762-8767.
[17] Murase, M.; Yabuuchi, N.; Han, Z.-J.; Son, J.-Y.; Cui, Y.-T.; Oji, H.; Komaba, S. Chemsuschem 5 (2012) 2307-2311.
[18] Hu, L.; La Mantia, F.; Wu, H.; Xie, X.; McDonough, J.; Pasta, M.; Cui, Y. Adv. Energy Mater. 1 (2011) 1012-1017.
[19] Gu, M.; Xiao, X.-C.; Liu, G.; Thevuthasan, S.; Baer, D. R.; Zhang, J.-G.; Liu, J.; Browning, N. D.; Wang, C.-M. Sci. Rep. 4 (2014).
[20] Xun, S.; Xiang, B.; Minor, A.; Battaglia, V.; Liu, G. J. Electrochem. Soc. 160 (2013) A1380-A1383.
[21] Buqa, H.; Holzapfel, M.; Krumeich, F.; Veit, C.; Novak, P. J. Power Sources 161 (2006) 617-622.
[22] Lux, S. F.; Schappacher, F.; Balducci, A.; Passerini, S.; Winter, M. J. Electrochem. Soc. 157 (2010) A320-A325.
[23] Jingu, K.; Kunhwi, K.; Yun Mook, L.; Bolander, J. E. Int. J. Solids Struct. 51 (2014) 1970-1979.
[24] Reed, M.; Lokuge, W.; Karunasena, W. J. Mater. Sci. 49 (2014) 4297-4304.
[25] Lam, L.; Teng, J. G. J. Struct. Eng-Asce 128 (2002) 612-623.
[26] Samaan, M.; Mirmiran, A.; Shahawy, M. J. Struct. Eng-Asce 124 (1998) 1025-1031.
[27] Maqbool, M.; Ali, A.; Alderson, P. G.; Mohamed, M. T. M.; Siddiqui, Y.; Zahid, N. Postharvest Biol. Tec. 62 (2011) 71-76.
[28] Ademoh, N. A. Int. J. Phys. Sci. 5 (2010) 557-563.
[29] Popoola, A. P. I. J. Sci. Ind. Res. 70 (2011) 1029-1032.
[30] Erk, C.; Brezesinski, T.; Sommer, H.; Schneider, R.; Janek, J. ACS Appl. Mater. Inter. 5 (2013) 7299-7307.
[31] Munao, D.; van Erven, J. W. M.; Valvo, M.; Garcia-Tamayo, E.; Kelder, E. M. J. Power Sources 196 (2011) 6695-6702.
[32] Tavakoli, H. R.; Omran, O. L.; Kutanaei, S. S.; Shiade, M. F. Lat. Am. J. Solids. Struct. 11 (2014) 966-979.
[33] Bakhshi, M.; Barsby, C.; Mobasher, B. Mater. Struct.47 (2014) 853-872.
[34] Ryu, J.; Ju, Y. K.; Yoon, S. W.; Kim, S. D. Mater. Res. Innovations 17 (2013) 12-18.
[35] Budiansky, B.; Hutchinson, J. W.; Evans, A. G. J. Mech. Phys. Solids. 34 (1986) 167-189.
[36] Marshall, D. B.; Evans, A. G. J. Am. Ceram. Soc. 68 (1985) 225-231.
[37] Magasinski, A.; Zdyrko, B.; Kovalenko, I.; Hertzberg, B.; Burtovyy, R.; Huebner, C. F.; Fuller, T. F.; Luzinov, I.; Yushin, G. ACS Appl. Mater. Inter. 2 (2010) 3004-3010.
[38] Yabuuchi, N.; Shimomura, K.; Shimbe, Y.; Ozeki, T.; Son, J.-Y.; Oji, H.; Katayama, Y.; Miura, T.; Komaba, S. Adv. Energy Mater. 1 (2011) 759-765.

[39] Cho, Y.-G.; Kim, Y.-S.; Sung, D.-G.; Seo, M.-S.; Song, H.-K. Energy Environ. Sci. 7 (2014）1737-1743.
[40] Zhian, Z.; Tao, Z.; Yanqing, L.; Ming, J.; Jie, L. J. Power Sources 247 (2014）1-8.
[41] Chen, J.; Liu, J.; Qi, Y.; Sun, T.; Li, X. J. Electrochem. Soc. 160 (2013）A1502-A1509.
[42] Liu, G.; Zheng, H.; Song, X.; Battaglia, V. S. J. Electrochem. Soc. 159 (2012）A214-A221.
[43] Lestriez, B.; Bahri, S.; Sandu, I.; Roue, L.; Guyomard, D. Electrochem. Commun. 9 (2007）2801-2806.
[44] Park, H.-K.; Kong, B.-S.; Oh, E.-S. Electrochem. Commun. 13 (2011）1051-1053.
[45] Espinosa-Andrews, H.; Sandoval-Castilla, O.; Vazquez-Torres, H.; Jaime Vernon-Carter, E.; Lobato-Calleros, C. Carbohydr. Polym. 79 (2010）541-546.
[46] Park, Y.; Lee, S.; Kim, S.-H.; Jang, B. Y.; Kim, J. S.; Oh, S. M.; Kim, J.-Y.; Choi, N.-S.; Lee, K. T.; Kim, B.-S. Rsc Adv. 3 (2013）12625-12630.
[47] Zhang, S. S. J. Power Sources 162 (2006）1379-1394.
[48] Edstrom, K.; Gustafsson, T.; Thomas, J. O. Electrochim. Acta 50 (2004）397-403.
[49] Peled, E.; Menachem, C.; BarTow, D.; Melman, A. J. Electrochem. Soc. 143 (1996）L4-L7.
[50] Hui, W.; Chan, G.; Jang Wook, C.; Ill, R.; Yan, Y.; McDowell, M. T.; Seok Woo, L.; Jackson, A.; Yuan, Y.; Liangbing, H.; Yi, C. Nat. Nanotechnol. 7 (2012）310-315.